Inorganic Chemistry

pubs.acs.org/IC Article

Paramagnetic Molecular Semiconductors Combining Anisotropic Magnetic Ions with TCNQ Radical Anions

Ökten Üngör, Maylu Burrows, Tianhan Liu, Michael Bodensteiner, Yuwaraj Adhikari, Zhenqi Hua, Brian Casas, Luis Balicas, Peng Xiong, and Michael Shatruk*

Cite This: *Inorg. Chem.* 2021, 60, 10502–10512 Read Online

ACCESS | Metrics & More | Article Recommendations | Supporting Information

ABSTRACT: We report the synthesis, magnetic properties, and transport properties of paramagnetic metal complexes, $[Co(DMF)_4(TCNQ)_2](TCNQ)_2$ (**1**), $[La(DMF)_8(TCNQ)](TCNQ)_5$ (**2**), and $[Nd(DMF)_7(TCNQ)](TCNQ)_5$ (**3**) (DMF = *N*,*N*-dimethylformamide, TCNQ = 7,7,8,8-tetracyanoquinodimethane). All three compounds contain fractionally charged $TCNQ^{\delta-}$ anions ($0 < \delta < 1$) and mononuclear complex cations in which the coordination environment of a metal center includes several DMF molecules and one or two terminally coordinated $TCNQ^{\delta-}$ anions. The coordinated $TCNQ^{\delta-}$ anions participate in $\pi-\pi$ stacking interactions with noncoordinated $TCNQ^{\delta-}$ anions, forming columnar substructures that provide efficient charge-transporting pathways. As a result, temperature-dependent conductivity measurements demonstrate that all three compounds exhibit semiconducting behavior.

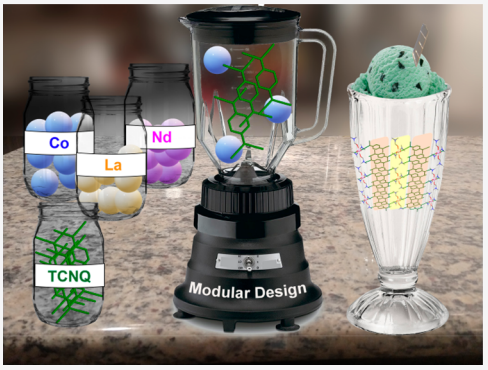

INTRODUCTION

The discovery of the TTF-TCNQ charge-transfer solid in 1973 was a major breakthrough in the field of organic conductors.[1,2] The crystal structure of this synthetic organic metal features segregated columns of TTF and TCNQ molecules. Partial electron transfer from the HOMO of TTF to the LUMO of TCNQ leads to fractionally charged radical cations and anions, with the formula of the material expressed as $(TTF)^{\delta+}(TCNQ)^{\delta-}$, where $\delta \approx 0.55$.[3] This compound shows high conductivity of 4×10^2 S/cm at room temperature, and the conductivity increases as the temperature is lowered, reaching 2×10^4 S/cm at 59 K, which is characteristic of a metallic material. Below this temperature, however, TTF-TCNQ becomes an insulator owing to Peierls transitions occurring independently in the TTF and TCNQ chains.

This seminal discovery has led to the synthesis and studies of many other molecular conductors based on TTF, TCNQ, and their derivatives, culminating in the discovery of the first organic superconductors in the 1980s.[4−6] Additionally, the possibility of combining organic radicals derived from the donor or acceptor molecules, such as TTF and TCNQ, respectively, and transition or lanthanide metal ions have also been a topic of extensive investigation.[7−11] The preferred columnar stacking of these organic molecules typically leads to quasi-one-dimensional (1D) molecular solids with strongly anisotropic conducting behavior, while the addition of the metal ions might impart interesting magnetic and optical behavior, as relevant to the development of multifunctional molecular materials.[12−17]

Besides forming efficient charge-transporting pathways, polynitrile acceptors, such as TCNQ (Scheme 1), can act as effective divergent bridging ligands, often leading to fast precipitation of amorphous or poorly crystalline coordination polymers in the reactions of integer-charged $TCNQ^-$ or fractionally charged $TCNQ^{\delta-}$ anions ($0 < \delta < 1$) with open-shell transition metal cations.[18,19] This problem can be overcome by the use of blocking ligands or coordinating solvents that compete with the coordination of TCNQ to the metal center. The use of blocking ligands can be especially effective to prevent the growth of extended metal-TCNQ coordination polymers,[15] and recently, we and others have

Scheme 1. Structure of TCNQ, the Famous Organic Acceptor Used in Preparation of Organic Metals

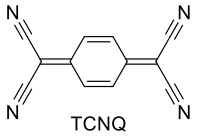

Received: April 13, 2021
Published: June 30, 2021

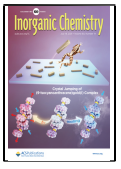

https://doi.org/10.1021/acs.inorgchem.1c01140
Inorg. Chem. 2021, 60, 10502−10512

successfully used this strategy to prepare molecular semiconductors with spin-state switching properties.[20−23]

A less obvious yet synthetically straightforward approach to avoid rapid precipitation of the extended metal-TCNQ structures is the use of readily available coordinating solvents as blocking ligands. Such an approach, however, is also more challenging, as one has to balance the coordinating ability of TCNQ and solvent molecules. There is a handful of reported crystal structures of coordination compounds in which solvent molecules and TCNQ anions are simultaneously coordinated to a paramagnetic metal center, although these examples are dominated by complexes of lanthanide ions (Table 1). The majority of these structures, however, contain integer-charged $TCNQ^-$ anions, and, therefore, the materials are expected to behave as insulators. Indeed, it is well established that higher conductivity in the organic substructure is promoted by creating fractionally charged cation- or anion-radicals derived from organic donor or acceptor molecules, respectively.[24,25]

Table 1. Transition Metal and Lanthanide Complexes That Contain Only the Solvent Molecules and $TCNQ^-$ or $TCNQ^{\delta-}$ Anions ($0 < \delta < 1$) as Co-Ligands

Formula	Structure Features of TCNQ
Complexes with Fractionally Charged TCNQ	
$[Fe(DMF)_4(TCNQ)_2](TCNQ)_2$[26]	Infinite 1D stacks of $TCNQ^{\delta-}$
$[Fe(MeOH)_4(TCNQ)_2](TCNQ)\cdot 2MeCN$[27]	Infinite 1D stacks of $TCNQ^{\delta-}$
Complexes with Integer Charged TCNQ	
3D Coordination Polymers	
$[Gd_2(DMF)_4(H_2O)_{12}(TCNQ)_2](TCNQ)_4\cdot 2DMF$[28]	1D stacks
$[Gd(DMTCNQ)_2(MeOH)(H_2O)_6](DMTCNQ)\cdot 4H_2O$[29]	1D stacks of $DMTCNQ^-$
$[Gd(DETCNQ)_2(H_2O)_7](DETCNQ)_2$[29]	1D stacks of $DETCNQ^-$
$[Gd_2(TCNQ)_4\ MeOH)_2(H_2O)_8](TCNQ)_2)\cdot 2H_2O$[30]	μ_2-, μ_3- and μ_4-$TCNQ^-$
$[Ce_2(TCNQX_2)_4(MeOH)_9(H_2O)](TCNQX_2)_2$ (X = Cl, Br)[31]	μ_2-$TCNQX_2^-$ bridging
2D Coordination Polymers	
$\{[Gd_2(TCNQ)_5(H_2O)_9][Gd(TCNQ)_4(H_2O)_3]\}\cdot 4H_2O$[28]	μ_2-, μ_3- and μ_4-$TCNQ^-$
$[Gd_2(TCNQ)_2(DMF)_4(H2O)_{12}](TCNQ)_4\cdot 4H_2O$[30]	1D stacks
$[Gd(TCNQ)_2(H_2O)_7](TCNQ)\cdot 6H_2O\cdot EtOH$[30]	1D stacks
$[Ln_2(TCNQ)_4(H_2O)_{10}](TCNQ)_2\cdot yH_2O$ (Ln = Gd, Dy, y = 6, 5)[32]	1D stacks
$[Ln_2(TCNQ)_4(EtOH)_2(H_2O)_{10}](TCNQ)_2\cdot nH_2O$ (Ln = La, Pr; n = 5, 3)[32]	1D stacks
Mono- and Dinuclear Complexes	
$[Ln(H_2O)_x(TCNQF_4)_2](TCNQF_4)\cdot 3H_2O$ (Ln = Y, La−Gd, Dy−Er, Yb; x = 6 or 7)[33]	$(TCNQF_4)_2^{2-}$ dimers
$[Ln(TCNQ)_2(H_2O)_6](TCNQ)\cdot H_2O\cdot 2MeOH$ (Ln = Ho, Yb)[30]	1D stack
$[Ln(TCNQ)_2(H_2O)_6](TCNQ)\cdot H_2O\cdot MeOH$ (Ln = Er, Lu)[32]	1D stacks
$[Ln(TCNQ)_2(H_2O)_7](TCNQ)\cdot 5H_2O\cdot EtOH$ (Ln = Nd, Sm, E, Gd)[34]	1D stacks
$[Ln_2(TCNQ)_2(H2O)_{15}](TCNQ)_4\cdot n(p\text{-dioxane})\cdot 7H_2O$ (Ln = Ce, Pr, Nd; n = 2.5, 2.5, 2)[34]	1D stacks
$[Ce_2(TCNQ)_4(MeOH)_2(H_2O)_{10}](TCNQ)_2\cdot 2H_2O\cdot 2MeOH$[31]	1D stacks

Following on these ideas, we have recently demonstrated the synthesis and crystal structure of $[Fe(DMF)_4(TCNQ)_2](TCNQ)_2$.[26] In the structure of this material, the octahedral coordination environment of the Fe^{II} ion consists of four equatorially coordinated DMF molecules and two axially coordinated $TCNQ^{\delta-}$ anions. The latter interact with free, noncoordinated $TCNQ^{\delta-}$ anions to form 1D stacks of fractionally charged TCNQ units with $\delta_{av} = 0.5$. This material showed high room-temperature (r.t.) conductivity of 0.12 S/cm, although the conductivity decreased at lower temperatures, characteristic of a paramagnetic semiconductor. A similar crystal packing was observed in an incidentally isolated complex, $[Fe(MeOH)_4(TCNQ)_2](TCNQ)\cdot 2MeCN$.[27] Nevertheless, despite $\delta_{av} = 0.67$, the coordinated and noncoordinated TCNQ units exhibit charges of −1 and 0, respectively, which suggests the material is likely to be insulating. To the best of our knowledge, these two complexes are the only examples of structurally characterized compounds that contain solely solvent molecules and fractionally charged TCNQ anions coordinated to paramagnetic metal centers.

Our interest in the coupling between the magnetic and conducting properties of such solids led us to investigate cocrystallization of *fractionally charged* $TCNQ^{\delta-}$ anions with more magnetically anisotropic 3d and 4f metal ions in the absence of blocking ligands. On the one hand, examples of structurally characterized materials of such type remain rare for 3d metal ions and unknown for 4f metal ions. On the other hand, the introduction of magnetically anisotropic metal ions can lead to the observation of conducting behavior due to the substructure formed by the $TCNQ^{\delta-}$ anions being combined with interesting magnetic properties, such as magnetic ordering or single-ion magnet (SIM) behavior. Herein, we describe the synthesis, crystal structures, and magnetic and transport properties of three new complexes, $[Co(DMF)_4(TCNQ)_2](TCNQ)_2$ (**1**), $[La(DMF)_8(TCNQ)](TCNQ)_5$ (**2**), and $[Nd(DMF)_7(TCNQ)](TCNQ)_5$ (**3**). The La- and Nd-containing complexes are the first examples of structurally characterized complexes between trivalent lanthanide cations and fractionally charged $TCNQ^{\delta-}$ anions, crystallized in the absence of any blocking ligands.

RESULTS AND DISCUSSION

Synthesis. In the previous reports (see Table 1), Ln-TCNQ complexes were synthesized by combining solutions of LiTCNQ and a metal precursor; this approach unavoidably resulted in materials with integer-charged $TCNQ^-$ anions. The only series of Ln complexes with fractionally charged $TCNQ^{\delta-}$ anions were reported by the Dunbar group,[35] who reacted $(Et_3NH)(TCNQ)_2$, in which TCNQ is already fractionally charged, and Ln^{3+} ions partially blocked with a tetradentate ligand tris(2-pyridylmethyl)amine (tpma) to obtain semiconducting chain compounds $\{[Ln(tpma)(\mu\text{-}OH)(\mu\text{-}TCNQ)](TCNQ)_2\cdot CH_3CN\}$ (Ln = Y, Gd, Dy). We used the same TCNQ precursor to obtain the semiconducting material $[Fe(DMF)_4(TCNQ)_2](TCNQ)_2$ mentioned above, albeit in the absence of any blocking ligands.[26] Here, we extend this synthetic strategy for the synthesis of three new metal complexes with fractionally charged $TCNQ^{\delta-}$ anions.

The reaction between $Co(BF_4)_2\cdot 6H_2O$ and $(Et_3NH)(TCNQ)_2$ in the 1:1.5 molar ratio afforded mononuclear complex **1**. Slow diffusion of Et_2O into the DMF solution of the complex afforded crystals of **1** as air-stable dark-green elongated plates. The TGA measurements (Figure S1a)

https://doi.org/10.1021/acs.inorgchem.1c01140
Inorg. Chem. 2021, 60, 10502−10512

showed that the complex began to lose its mass upon heating. The mass loss reached 14.0% by 100 °C, which corresponds to the loss of three coordinated DMF molecules per formula unit (f.u.). At higher temperatures, the mass loss continued in two steps, due to the loss of the remaining DMF molecule and the decomposition of TCNQ anions. An additional decomposition step was observed upon further heating to 400 °C.

Complexes **2** and **3** were obtained by the reactions between the corresponding lanthanide salt, $La(NO_3)_3{\cdot}6H_2O$ or $NdCl_3$, and $(Et_3NH)(TCNQ)_2$ in the 1:2 molar ratio. Both complexes crystallize as air-stable dark-blue needles. The TGA measurements revealed that complex **2** is thermally stable up to 200 °C, above which two sequential decomposition steps take place (Figure S1b). In contrast, complex **3** shows a 5% mass loss at 50 °C, which can be attributed to the loss of one DMF molecule per f.u. The mass loss reaches 22% at 140 °C, corresponding to the total loss of seven DMF molecules. Decomposition of the complex is observed at higher temperatures (Figure S1c).

Crystal Structure. The crystal structures of complexes **1**−**3** were determined at 150 K. Complex **1** crystallizes in the space group $P\bar{1}$. It is isomorphous to the compound $[Fe(DMF)_4(TCNQ)_2](TCNQ)_2$ already reported by us.[26] The asymmetric unit (Figure S2) consists of one mononuclear cation, $[Co(DMF)_4(TCNQ)_2]^{2(1-\delta)+}$, and two noncoordinated $TCNQ^{\delta-}$ anions. Each Co^{2+} ion in the cationic complex is octahedrally coordinated by oxygen atoms of four DMF molecules in the equatorial positions and two nitrogen atoms of $TCNQ^{\delta-}$ anions in the axial positions. The average Co−O and Co−N bond lengths are 2.075(1) Å and 2.112(2) Å, respectively.

The most notable feature of the crystal structure of **1** is infinite one-dimensional stacks of TCNQ units, which propagate along the crystallographic *b* direction (Figures 1 and 2a). In these stacks, pairs of the noncoordinated $TCNQ^U$ anions alternate with pairs of the $TCNQ^C$ anions that are terminally coordinated to the Co^{II} centers of the mononuclear cations. The interplanar distances between the TCNQ units along this [UCCU] repeat pattern (Figure 2b) are 3.100, 3.213, 3.133, and 3.298 Å, where the last number refers to the distance to the next repeat unit. The $TCNQ^C$−$TCNQ^U$ π−π overlaps are of the ring-external bond type, and the $TCNQ^C$−$TCNQ^C$ and $TCNQ^U$−$TCNQ^U$ overlaps are of the ring-over-ring type. The electroneutrality requirement results in the average charge of −0.50 per TCNQ anion in **1**. The charge on each TCNQ unit was estimated from the Kistenmacher relationship,[36] using the bond lengths in TCNQ established by the crystal structure analysis and scaling the obtained charges to conform to the electroneutrality of the material (see Table S1 and the accompanying description). These calculations led to charges on $TCNQ^C$ and $TCNQ^U$ being equal to −0.65 and −0.35, respectively. Such an uneven charge distribution on the TCNQ units was also observed in the previously reported Fe(II) analog,[26] where the charges on $TCNQ^C$ and $TCNQ^U$ were equal to −0.74 and −0.35. Given the similarity of the crystal packing and charge distribution in the two complexes, it can be expected that the Co-containing complex **1** should exhibit appreciable conductivity, similar to what was observed for the Fe-containing analog.

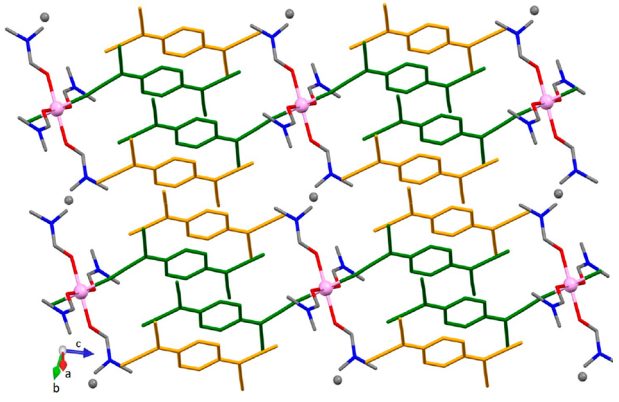

Figure 1. Crystal structure of **1**. The color scheme: Co = light purple, O = red, *N* = blue, C = gray, $TCNQ^C$ = green, $TCNQ^U$ = orange. The H atoms are omitted for clarity. The gray spheres indicate the location of disordered Co sites. See the text for further discussion.

One may notice that the average charge per TCNQ anion in complex **1**, $-\delta_{av} = -1/2 \times (0.65 + 0.35) = -0.50$, while in the Fe-containing analog, $-\delta_{av} = -1/2 \times (0.74 + 0.35) = -0.545$. The reason for this discrepancy is an observation of a large residual electron density (r.e.d.) peak in the crystal structure of the Fe-containing complex. Indeed, we observed the presence of a similar peak in the difference Fourier electron density map in the structure refinement for complex **1** (the gray circles in Figure 1). In the previous publication, we tentatively attributed such a peak to a crystallographic site partially occupied by Na^+ ions, as the latter are well-known to be omnipresent in chemical reactions carried out in glass containers. Nevertheless, the relatively good yield of the crystals of the Fe-TCNQ or Co-TCNQ complexes makes this hypothesis questionable, as it is unlikely that such a large amount of Na^+ ions could be etched out from the container walls under relatively mild reaction conditions. Here, we present a new, more realistic model of this crystal structure, which rules out the possible presence of adventitious alkali metal ions in these crystal structures.

Single crystals of **1** were subjected to energy-dispersive X-ray (EDX) microanalysis, which revealed that the amount of Na in the sample was negligible. Given this finding, we can rule out the assignment of the r.e.d. peak to the partially occupied Na site. The availability of higher-quality X-ray diffraction data, obtained with a newer state-of-the-art diffractometer equipped with a Cu-Kα microfocus radiation source (see the Materials and Methods section), allowed observation of more r.e.d. peaks around the main r.e.d. peak (Figure S2). These peaks clearly revealed the presence of another orientation of the coordinated DMF molecules, thus hinting that the largest r.e.d. peak simply corresponded to the disorder of the entire $[Co(DMF)_4]$ structural fragment, where the second, less occupied position of the Co^{2+} ion, appeared exactly in the middle between two symmetry-equivalent positions corresponding to the major Co^{2+} site. This disorder model satisfactorily converged to the low value of *R*-factor and residual maximum and minimum electron density peaks. Therefore, with these new data in hand, it becomes obvious that the correct assignment of the average oxidation state per $TCNQ^{\delta-}$ anion should be $-\delta_{av} = -0.5$, for both complex **1** and its Fe(II) analogue reported earlier.[26] Interestingly, the observed disorder might be invoked to understand the observation of a small ionic contribution to conductivity, as will be discussed in the Transport Properties section below.

Complex **2** also crystallizes in the space group $P\bar{1}$. Although the structural motif is similar to that of complex **1**, the

https://doi.org/10.1021/acs.inorgchem.1c01140
Inorg. Chem. 2021, 60, 10502−10512

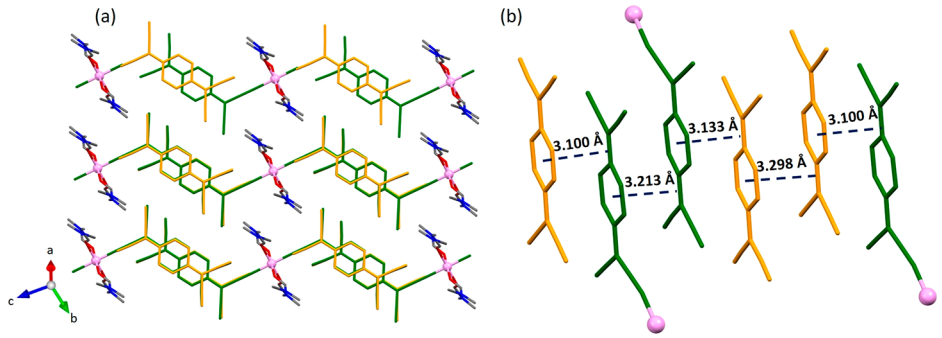

Figure 2. (a) Top view of the 1D stacks of TCNQ units in the crystal structure of **1**. (b) Side view of a single stack of TCNQ units, with the indication of interplanar distances. Color scheme: Co = light purple, O = red, *N* = blue, C = dark gray, $TCNQ^{C}$ = green, $TCNQ^{U}$ = orange.

coordination environment and the packing of TCNQ units in the crystal structure are rather different. The asymmetric unit consists of a mononuclear cationic complex $[La(DMF)_8(TCNQ)]^{(3-\delta)+}$ and five noncoordinated TCNQ anions ($TCNQ^{U}$) (Figure 3). The nine-coordinate environment of the La^{3+} ion is composed of eight oxygen-bound DMF molecules and one N-bound TCNQ anion ($TCNQ^{C}$). The O atoms of DMF molecules form a square-antiprismatic coordination around the La^{3+} ions, while the N atom of TCNQ completes the coordination by capping one of the square faces of the antiprism. Such a geometry is also reflected in the longer value of the La−N bond length, 2.851(2) Å, as compared to the La−O bond lengths, which vary from 2.471(2) to 2.579(2) Å.

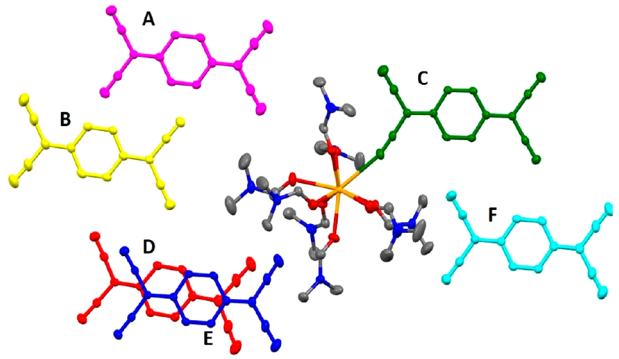

Figure 3. Asymmetric unit of **2** showing the mononuclear $[La(DMF)_8(TCNQ)]^{(3-\delta)+}$ cation and five $TCNQ^{\delta-}$ anions. Different colors are used to label crystallographically distinct TCNQ units. The color scheme for other atoms: La = orange, O = red, *N* = blue, C = gray. The H atoms are omitted for clarity. The thermal ellipsoids are at the 50% probability level.

In the crystal structure of **2**, two types of 1D stacks of TCNQ units were observed, both of which propagate along the *b* axis (Figure 3b). The first type of stacks includes both $TCNQ^{C}$ and $TCNQ^{U}$ units, forming the repeating pattern [CABCAB]. The interplanar TCNQ−TCNQ distances along the repeat unit are 3.212, 3.269, 3.303, 3.298, 3.223, and 3.328 Å, with the last value referring to the distance to the next repeat unit. The second type of stacks only includes the $TCNQ^{U}$ units that form the repeating pattern [FEDFED], with the interplanar distances of 3.283, 3.214, 3.257, 3.294, 3.207, and 3.257 Å. The overlap between $TCNQ^{C}$−$TCNQ^{U}$ is of the ring-external bond type, and the $TCNQ^{C}$−$TCNQ^{C}$ and $TCNQ^{U}$−$TCNQ^{U}$ overlaps are of the ring-over-ring type.

The average charge per TCNQ anion in complex **2** is equal to −0.50. The Kistenmacher relationship was used to assign charges to each crystallographically unique TCNQ anion, A through F, resulting in charges of−0.40, −0.65, −0.50, −0.50, −0.40, and −0.40, respectively. These values indicate that the charge distribution over the TCNQ anions in complex **2** is more uniform as compared to the charge distribution observed in complex **1** or its Fe(II) analog (Figure 4).

Lastly, complex **3** crystallizes in the space group $P\bar{1}$, with the asymmetric unit containing a mononuclear cationic complex $[Nd(DMF)_7(TCNQ)]^{(3-\delta)+}$ and five TCNQ anions ($TCNQ^{U}$, each denoted as described for complex **2**) (Figure 5). The eight-coordinate environment of the Nd^{3+} ion consists of seven O-bound DMF molecules and one N-bound TCNQ anion ($TCNQ^{C}$). The coordination geometry can be described as a trigonal prism composed of six O atoms of DMF molecules, with the O atom of the remaining DMF molecule and the N atom of the $TCNQ^{C}$ anion capping two sides of the prism. The

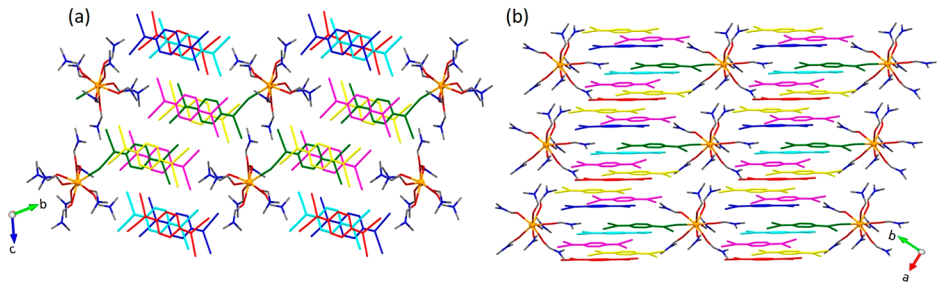

Figure 4. (a) The top view of the one-dimensional stacks of $TCNQ^{\delta-}$ anions in the crystal packing of **2**. (b) The side view of the $\pi-\pi$ stacking between $TCNQ^{\delta-}$ anions in **2**. Different colors are used to label crystallographically distinct TCNQ units. The color scheme for other atoms: La = orange, O = red, *N* = blue, C = gray. Hydrogen atoms are omitted for clarity.

https://doi.org/10.1021/acs.inorgchem.1c01140
Inorg. Chem. 2021, 60, 10502−10512

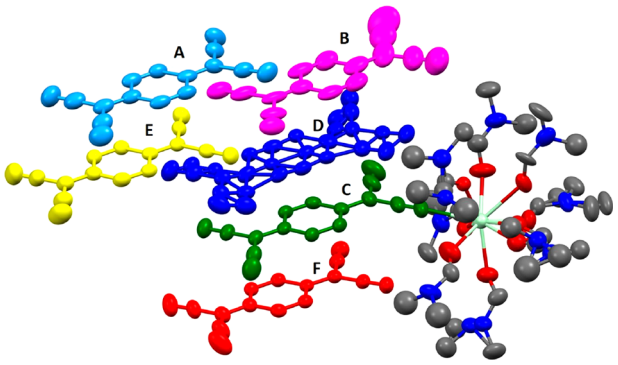

Figure 5. Asymmetric unit of **3** showing the mononuclear $[Nd(DMF)_7(TCNQ)]^{(3-\delta)+}$ cation and five $TCNQ^{\delta-}$ anions. Different colors are used to label crystallographically distinct TCNQ units. The color scheme for other atoms: Nd = orange, O = red, *N* = blue, C = gray. For clarity, the H atoms are omitted and only one component is shown for each disordered molecular fragment. The thermal ellipsoids are at the 50% probability level.

Nd−N bond length is 2.672(1) Å while the Nd−O bond lengths range from 2.344(8) to 2.453(8) Å.

Interestingly, the difference of one DMF molecule in the coordination environment of the lanthanide ion leads to substantial differences in the crystal packing of complexes **2** and **3**. First of all, the coordinated DMF molecules show substantial disorder that can be explained by the decreased density of the coordination sphere around the Nd^{3+} center. Second, only one type of 1D stacks of TCNQ units is observed in the crystal structure of **3** (Figure 6). The stacks form the repeating sequence [ABCDEF] along the *a* axis, with the TCNQ−TCNQ interplanar distances of 3.203, 3.284, 3.153, 3.333, 3.262, and 3.331 Å. The $TCNQ^C$−$TCNQ^U$ overlaps are of the ring-over-ring type, and the $TCNQ^C$−$TCNQ^C$ and $TCNQ^U$−$TCNQ^U$ overlaps are of the ring-over-external-bond type. The average charge per TCNQ anion in **3** is equal to −0.50, while the charges calculated from the Kistenmacher equation are −0.20, −1, −0.70, −0.25, −0.55, and −0.35 for the TCNQ units A through F, respectively.

Complexes **2** and **3** represent the first examples of structurally characterized lanthanide-TCNQ materials that contain fractionally charged $TCNQ^{\delta-}$ anions and lack any capping ligands besides the coordinated solvent molecules. The only other series of structurally characterized lanthanide complexes with fractionally charged $TCNQ^{\delta-}$ anions are already mentioned $\{[Ln(tpma)(OH)(TCNQ)](TCNQ)_2 \cdot CH_3CN\}_\infty$ (Ln = Y, Gd, Dy) whose structures include the tetradentate capping ligand, tpma.[35] These complexes were shown to exhibit semiconducting properties, and, therefore, similar transport behavior can be expected for materials **2** and **3**.

Infrared Spectroscopy. The infrared (IR) spectra of complexes **1**−**3** revealed characteristic peaks in the 2100−2250 cm^{-1} region due to the stretching vibrations of the nitrile groups. The IR peaks in this region were observed at ν_{CN} (cm^{-1}) of 2217, 2214, and 2155 for complex **1**, 2214, 2213, and 2150 for complex **2**, and 2215, 2214, and 2156 for complex **3**. Chappell et al. established a relationship between the ν_{CN} value and the charge on the $TCNQ^{\delta-}$ anion, $\nu_{CN} = 2227-44\delta$ (cm^{-1}),[37] according to which the neutral TCNQ molecule and the $TCNQ^-$ monoanion exhibit ν_{CN} stretches at 2227 and 2183 cm^{-1}, respectively. Therefore, two of the stretches observed for each of complexes **1**−**3** fall within a reasonable range for fractionally charged $TCNQ^{\delta-}$ moieties, but the third stretch for each complex is observed at a substantially lower energy than the stretch expected for $\delta = 1$. The reason for this discrepancy is the presence of coordinated nitrile groups in structures **1**−**3**. Indeed, the dependence of ν_{CN} on δ was derived empirically by considering only compounds with noncoordinated $TCNQ^{\delta-}$ anions. The σ-donation from the coordinating nitrile to the metal cations causes the simultaneous weakening of the C≡N bond and the decrease in its stretching frequency. For the same reason, while it is tempting to use the relationship above to estimate the values of δ for each complex, such an assignment is problematic due to the presence of both coordinated and noncoordinated TCNQ units in the crystals structures of **1**−**3** and the existence of multiple nonequivalent TCNQ units, especially in the structures of **2** and **3**.

Magnetic Properties. The magnetic properties were investigated on polycrystalline samples of complexes **1**−**3**. As expected, complexes **1** and **3** exhibit paramagnetic behavior, while complex **2** shows very weak paramagnetism. The product of magnetic susceptibility (χ) by temperature (T) for complex **1** gradually decreases from χT = 2.35 emu·K/mol at 300 K to 1.31 emu·K/mol at 1.8 K (Figure 7a). The temperature dependence of inverse magnetic susceptibility above 100 K was fit to the Curie−Weiss law, $1/\chi = (T - \theta)/C$, resulting in the Curie constant C = 2.61(1) emu·K/mol and the Weiss constant θ = −29.8(2) K (Figure 7b). The value of C is substantially larger than the spin-only value of 1.875 emu·K/mol expected for the high-spin (HS) Co^{2+} ion ($3d^7$, $S = 3/2$),

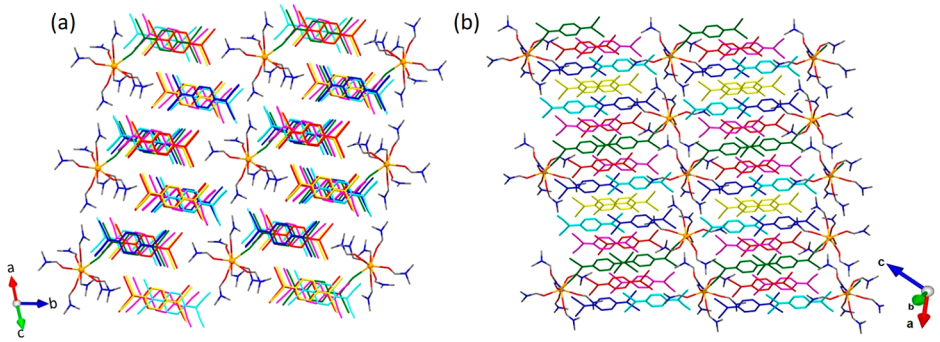

Figure 6. (a) The top view of the one-dimensional stacks of $TCNQ^{\delta-}$ anions in the crystal packing of **3**. (b) The side view of the π−π stacking between $TCNQ^{\delta-}$ anions. Different colors are used to label crystallographically distinct TCNQ units. The color scheme for other atoms: Nd = orange, O = red, *N* = blue, C = gray. Hydrogen atoms are omitted for clarity.

https://doi.org/10.1021/acs.inorgchem.1c01140
Inorg. Chem. 2021, 60, 10502−10512

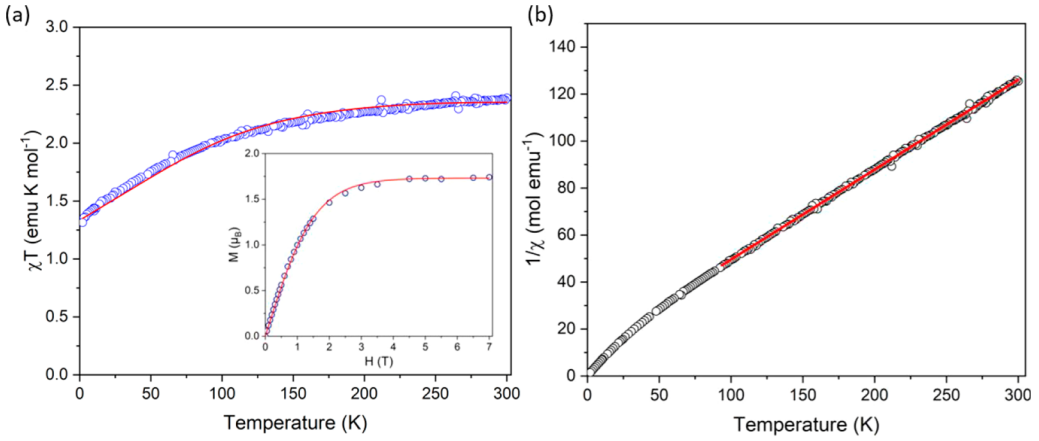

Figure 7. Temperature dependence of χT (a) and $1/\chi$ (b) for complex **1**. The inset in panel a shows the field dependence of magnetization measured at 1.8 K. The solid red lines in panels a and b show the fits to the corresponding theoretical models, as explained in the text.

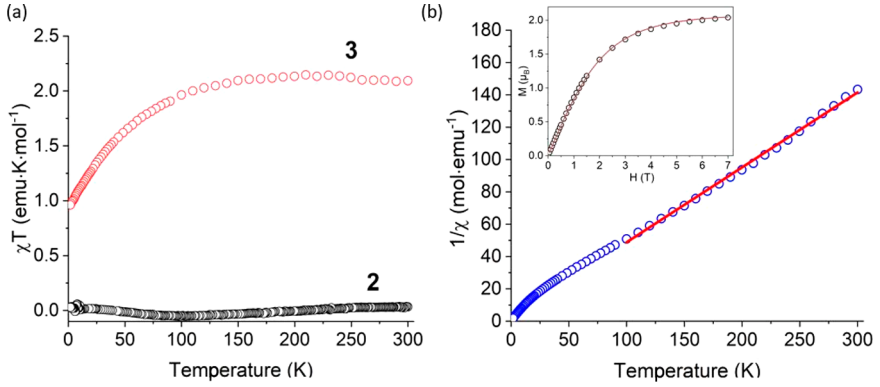

Figure 8. (a) The temperature dependence of χT for complexes **2** (black) and **3** (red). (b) The Curie−Weiss fit (solid red line) of the inverse magnetic susceptibility for complex **3** and the field dependence of magnetization measured at 1.8 K (inset).

but such deviation is well-known to occur in HS Co^{2+} complexes due to the significant orbital contribution to the total magnetic moment. Furthermore, the large negative value of θ and the gradual decrease in the χT value with temperature stem from strong spin−orbit coupling characteristic of the octahedrally coordinated HS Co^{2+} ion,[38] rather than from strong antiferromagnetic exchange interactions. Indeed, as was observed for the isomorphous Fe^{2+} complex, the magnetic exchange interactions in this type of structure are weak.[26] Thus, the effect of the magnetic exchange coupling cannot be estimated directly from the χT curve observed for complex **1**, since the spin−orbit coupling effects are dominant in this compound.

The temperature dependence of χT for a mononuclear octahedral Co(II) complex can be fit explicitly by considering the spin−orbit split microstates of the ^4F and ^4P terms and deriving the expression for χT via the general Van Vleck equation, as was demonstrated by Lloret et al.[39] The corresponding Hamiltonian is expressed as a sum of the Zeeman and spin−orbit coupling terms:

$$\hat{\mathcal{H}} = (-\alpha\hat{L} + g_e\hat{S})\mu_B\vec{B} - \alpha\lambda\hat{L}\hat{S} \quad (1)$$

where $g_e \approx 2$ is the Lande g-factor for a free electron, α is the orbital reduction factor, λ is the spin−orbit coupling constant, μ_B is the Bohr magneton, $\vec{B}$ is the applied magnetic field, and $\hat{L}$ and $\hat{S}$ are the operators of the orbital and spin angular momenta, respectively. By acting with this Hamiltonian on the free-ion ground and first excited states and entering the energies of resulting microstates into the Van Vleck equation, one obtains the following expression for χT:

$$\chi T = \frac{N\mu_B^2}{\lambda}\frac{F_1}{F_2} \quad (2)$$

where

$$F_1 = \frac{7\lambda}{5kT}(3-\alpha)^2 + \frac{12(2+\alpha)^2}{25\alpha} + \left[\frac{2\lambda}{45kT}(11-2\alpha)^2 + \frac{176(2+\alpha)^2}{675\alpha}\right]\exp\left(-\frac{5\alpha\lambda}{2kT}\right) + \left[\frac{\lambda}{9kT}(5+\alpha)^2 - \frac{20(2+\alpha)^2}{27\alpha}\right]\exp\left(-\frac{4\alpha\lambda}{kT}\right) \text{ and}$$

$$F_2 = 3 + 2\exp\left(-\frac{5\alpha\lambda}{2kT}\right) + \exp\left(-\frac{4\alpha\lambda}{kT}\right)$$

Using eq 2, the best fit to the temperature dependence of χT for complex **1** (Figure 7a) was obtained with the parameters $\lambda = -403(3)$ cm^{-1} and $\alpha = 0.660(3)$ ($R^2 = 0.9935$). While the value of α is close to the range typically observed for high-spin Co(II) complexes, the value of λ is nearly twice as large as the typical values observed for the high-spin Co(II) ion.[39] The reason for such an anomaly is the oversimplification introduced in the present model by ignoring the effects of

https://doi.org/10.1021/acs.inorgchem.1c01140
Inorg. Chem. 2021, 60, 10502−10512

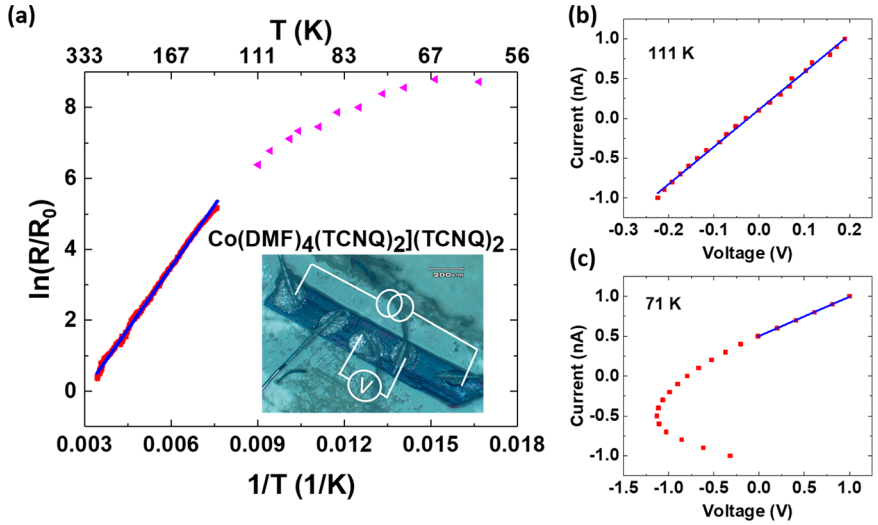

Figure 9. (a) A plot of $\ln(R/R_0)$ vs $1/T$ for a single crystal of **1**. The triangles represent resistances determined from individual *I-V* measurements at low temperatures. The blue solid line is a linear fit to the high-temperature data, which yields an activation energy E_a = 100 meV. Inset: Optical image of the crystal with five silver paint contacts and a schematic of the four-terminal measurement setup. (b, c) The *I-V* curves measured at 111 and 71 K, respectively. The resistance was calculated from these curves using the linear fits shown with solid blue lines.

magnetic exchange interactions between the Co(II) ions in the structure of **1**. This assumption led to the magnetic exchange coupling, which becomes more pronounced at lower temperatures, being effectively "absorbed" by the spin−orbit coupling constant.

The field-dependent magnetization curve measured at 1.8 K was fit to the Brillouin function (Figure 7a, inset), which was calculated taking into account that the ground state for the octahedral HS Co^{2+} ion is described by the effective spin value S_{eff} = 1/2 due to the spin−orbit splitting.[38] This fit resulted in g = 3.46(1), which is typical for the ground state of the Co(II) HS ion that behaves as an effective spin doublet at low temperatures.[38]

Trivalent lanthanide ions can exhibit large magnetic anisotropy arising from strong spin−orbit coupling. For that reason, these ions have been widely employed to prepare molecule-based magnets with organic radicals.[40] We investigated the magnetic properties of **2** and **3**, using the former as a model with the diamagnetic La^{3+} ion to evaluate the contribution of $TCNQ^{\delta-}$ anions to the magnetism of these compounds. The χT product of **2** remains nearly constant as a function of temperature (Figure 8a). The rather low value observed, ∼0.1 emu·K/mol, indicates that the $TCNQ^{\delta-}$ anions are only weakly magnetic in these materials. The reasons for the lack of a stronger magnetic contribution from these fractionally charged anions (expected at 0.375 emu·K/mol for an integer-charged $TCNQ^-$ radical) are two-fold. First, the antiferromagnetic exchange along the stack of anions can lead to the lower magnetic moments, but such an exchange would have to be exceptionally strong to decrease the χT value to nearly 0 at 300 K. Second, and more likely, the delocalized nature of charge carriers caused by increased electrical conductivity also leads to the decreased magnetic moments. It was shown previously that, as the conductivity of a material based on organic radicals increases, the electron paramagnetic resonance (EPR) signals become weaker, and, in general, the majority of organic conductors show very low EPR signals.[41]

The χT product of **3** shows a decrease from 2.10 emu·K/mol at 300 K to 0.98 emu·K/mol at 1.8 K (Figure 8a). The χT data above 100 K were fit to the Curie−Weiss law, resulting in the best-fit values of C = 2.16(2) emu·K/mol and θ = −5.37(3) K (Figure 8b). The value of C is somewhat higher than 1.65 emu·K/mol expected for a free Nd^{3+} ion ($4f^3$, J = 9/2, g = 8/11). The negative value of the Weiss constant indicates weak antiferromagnetic interactions between the Nd^{3+} ions and $TCNQ^{\delta-}$ radicals. Due to the fractional charge on the $TCNQ^{\delta-}$ radicals, it is difficult to evaluate their total contribution to the magnetization, but the antiferromagnetic exchange interactions clearly manifest themselves in the low-temperature behavior of this complex. Such interactions were also observed in related complexes (Table 1), such as $[Er(TCNQ)_2(H_2O)_6](TCNQ)\cdot H_2O\cdot MeOH$,[32] $[Gd(DETCNQ)_2(H_2O)_7](DETCNQ)_2$,[29] and $[Ce_2(TCNQCl_2)_4(MeOH)_9(H_2O)](TCNQX_2)_2$ (X = Cl, Br).[31] The field-dependent magnetization measured at 1.8 K does not saturate even at the highest field of 7 T attainable in our experiments. The magnetization reaches the maximum value of 2.0 μ_B, which is significantly lower than 3.28 μ_B expected for a single Nd^{3+} ion. Such dependence is also in agreement with antiferromagnetic exchange interactions dominating the low-temperature magnetic behavior of complex **3**.

Transport Properties. On the basis of the structural similarities with the previously reported Fe(II) analog, complex **1** is expected to show semiconducting properties with good electrical conductivity (σ). Indeed, the 4-probe conductivity measurements performed on a single crystal of **1** along the direction of TCNQ stack propagation revealed $\sigma = 7.6 \times 10^{-3}$ S/cm at 295 K, which is comparable to the values observed for other semiconducting materials obtained from the combination of transition metal complexes with fractionally charged $TCNQ^{\delta-}$ anions.[15]

Temperature-dependent measurements of transport properties are shown in Figure 9a as a logarithmic plot of the normalized sample resistance versus $1/T$. The resistance increases exponentially as the temperature decreases, confirming that **1** is a paramagnetic semiconductor. Isothermal *I-V* curves measured at higher temperatures (>130 K) were linear, and, therefore, the $R(T)$ dependence was obtained via standard 4-probe direct-current (DC) measurements. Below 110 K, the

https://doi.org/10.1021/acs.inorgchem.1c01140
Inorg. Chem. 2021, 60, 10502−10512

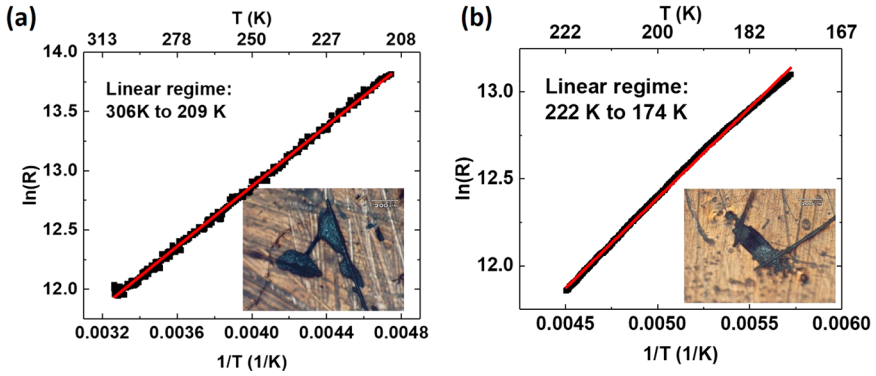

Figure 10. Linear regimes in the plots of ln(R) vs $1/T$ for **2** (a) and **3** (b). The resistance at higher temperatures exhibits a thermally activated behavior. The optical images of the crystals with two silver paint contacts are shown in the insets.

onset of the *I-V* curves showed a nonlinear behavior, which became more pronounced with decreasing temperature (Figure 9b,c). The nonlinearity appeared to be transient and could not be eliminated by reducing the current range of the *I-V* measurements (for details, see Figure S3). This nonlinear behavior might stem from a small *ionic* contribution to the sample conductance that becomes more noticeable at lower temperatures, after the decrease of the *electronic* conductance by a few orders of magnitude. Consequently, the low-temperature resistances data shown in Figure 9a were obtained by measuring the *I-V* dependence at each temperature point and determining the slope of the linear region (presumably, after the ionic transport has reached a steady state).

The dependence of resistance in the high-temperature region was fitted to the Arrhenius law, $\ln(R/R_0) = E_a/k_BT$, where R_0 is the resistance at 295 K, E_a is the activation energy for charge hopping, and k_B is the Boltzmann constant. The best-fit value of E_a was equal to 100 meV, which is lower than the value of 180 meV observed for the Fe-containing analog.[26] In contrast to the Fe(II) complex, which showed fast increase in the resistance over time due to deterioration of the crystals exposed to air, the crystals of **1** appear to remain stable for several hours, without any visible degradation or large changes in their resistivity.

Due to the smaller size of the crystals of **2** and **3**, conductivity of these complexes could not be measured with the 4-probe method. Therefore, we used a 2-probe setup to evaluate transport properties of these complexes. The room-temperature conductivity was found equal to 9.0×10^{-3} S/cm for **2** and 1.8×10^{-2} S/cm for **3**, although the contact resistance for these samples, probably, was non-negligible, and the intrinsic conductivity might be higher. The overall temperature dependence of resistance resembled that of **1** (Figure S4). The dependence of ln(R) on $1/T$ was fit to the Arrhenius equation in the well-defined thermally activated region observed at higher temperatures (Figure 10), resulting in E_a = 105 meV for **2** and 89 meV for **3**.

CONCLUDING REMARKS

We have shown that complexes of paramagnetic transition and lanthanide metal ions with fractionally charged $TCNQ^{\delta-}$ anions ($0 < \delta < 1$) can be efficiently crystallized from DMF solutions. This procedure takes advantage of the coordinating behavior of DMF, which plays the role of so-called "blocking ligands" to prevent fast precipitation of extended TCNQ-bridged structures. The stacks of $TCNQ^{\delta-}$ anions present in the structures of complexes **1**−**3** provide efficient charge transport pathways, leading to semiconducting behavior of these materials. Complex **1**, which contains an octahedrally coordinated Co^{II} ion, is isomorphous with the Fe^{II} complex previously reported by us. Interestingly, the Co^{II} ion shows slight crystallographic disorder, which might explain the observation of minor ionic contribution to the charge transport. In the case of the Fe^{II} complex, this disorder was also manifested in the observation of two distinct components in the Mössbauer spectrum of the material.

Extension of this synthetic approach to the lanthanide ions offers the pathway to the preparation of semiconducting materials with strongly anisotropic paramagnetic ions. Such materials might exhibit single-ion magnet and single-chain magnet behavior, depending on the specific ion used and the crystal packing achieved. Coupling such properties to the conductivity of the TCNQ substructure should yield multi-functional molecular solids with a potentially interesting synergy of properties, especially taking into account well-established luminescent properties of some lanthanide ions. We hope that our work will encourage further studies in this direction.

MATERIALS AND METHODS

Synthesis. All reactions were performed under an inert N_2 atmosphere using standard Schlenk techniques. All anhydrous solvents were purchased from Aldrich. TCNQ was obtained from TCI America, while the metal precursors, $Co(BF_4)_2{\cdot}6H_2O$, $La(NO_3)_3{\cdot}6H_2O$, and $NdCl_3$, were obtained from Alfa Aesar. All commercial reagents were used as received. $(Et_3NH)(TCNQ)_2$ was prepared according to the published procedure.[42] Elemental analysis was performed by Atlantic Microlab, Inc. (Norcross, GA, USA).

$[Co(DMF)_4(TCNQ)_2](TCNQ)_2$.[1] A 17.0 mg (0.050 mmol) portion of $Co(BF_4)_2{\cdot}6H_2O$ was dissolved in 1.0 mL of acetone. The obtained solution was added to a solution of 38.2 mg (0.075 mmol) of $(Et_3NH)(TCNQ)_2$ in 3.0 mL of DMF-acetone mixture (1:2 v/v). The resulting clear dark-green solution was stirred for 10 min, filtered, and layered by diethyl ether (Et_2O) for crystallization. Dark-green plate-like crystals were recovered by filtration, washed with Et_2O, and dried by suction. Yield = 31.0 mg (53%). IR(cm^{-1}), ν(C≡N): 2217, 2214, 2155; ν(C=N): 1505; ν(C−H): 835. Elemental analysis: Calcd (Found) for $CoO_4N_{20}C_{60}H_{44}$ (**1**), %: C 60.50 (60.68), N 23.69 (23.99), H 3.90 (3.80).

$[La(DMF)_7(TCNQ)](TCNQ)_5$ (2). 10.8 mg (0.025 mmol) of $La(NO_3)_3{\cdot}6H_2O$ was dissolved in 2.0 mL of a DMF-acetone mixture (1:1 v/v). This solution was added to a solution of 25.5 mg (0.050 mmol) of $(Et_3NH)(TCNQ)_2$ a in 2.0 mL of acetone. After stirring for 10 min, the resulting blue solution was filtered, layered by Et_2O, and left in the fridge (6 °C) for crystallization. Dark-green needle-like

https://doi.org/10.1021/acs.inorgchem.1c01140
Inorg. Chem. 2021, 60, 10502−10512

crystals that formed were recovered by filtration, washed with Et_2O, and dried by suction. Yield = 21.2 mg (45.2%). *IR*(cm^{-1}), ν(C≡N): 2213, 2214, 2150; ν(C=N): 1506; ν(C−H): 830. Elemental analysis: Calcd (Found) for $LaO_7N_{31}C_{93}H_{73}$ (**2**), %: C 59.55 (59.71), N 23.15 (23.45), H 3.92 (3.81).

[Nd(DMF)$_7$(TCNQ)](TCNQ)$_5$ (3). Compound **3** was prepared in a manner analogous to that described for **2**, using 11.0 mg (0.025 mmol) of $Nd(NO_3)_3{\cdot}6H_2O$ and with the same amounts of $(Et_3NH)(TCNQ)_2$ and solvent. Dark-blue needle-like crystals that formed were recovered by filtration, washed with Et_2O, and dried by suction. Yield = 20.0 mg (42.5%). *IR*(cm^{-1}), ν(C≡N): 2215, 2214, 2156; ν(C=N): 1500; ν(C−H): 838. Elemental analysis: Calcd (Found) for $NdO_7N_{31}C_{93}H_{73}$ (**3**), %: C 59.38 (59.79), N 23.08 (23.51), H 3.91 (3.83).

Physical Measurements. TGA was performed on the TA Instruments Q50 Thermogravimetric Analyzer, in the temperature range from 25 to 400 °C, at a heating rate of 5 °C/min. IR spectra were acquired in the range of 4000−400 cm^{-1} using a JASCO 6800 FT-IR spectrometer.

X-ray Crystallography. Single-crystal X-ray diffraction was performed on a Rigaku-Oxford Diffraction Synergy-S diffractometer equipped with a HyPix detector and a monochromated Cu-Kα (λ = 1.54184 Å for **1** and **3**) or Mo-Kα (λ = 0.71073 Å for **2**) radiation source. A chosen single crystal was suspended in Parabar oil (Hampton Research) and mounted on a cryoloop, which was cooled to the desired temperature in an N_2 cold stream. The data set was recorded using ω-scans at 0.5° step width and integrated with the CrysAlisPro software package, which was also used for space group determination.[43] An empirical absorption correction was applied based on spherical harmonics as implemented in the SCALE3 ABSPACK algorithm.[44] The crystal structure solution and refinement were carried out with SHELX[45] using the interface provided by Olex2.[46] The final refinement was performed with anisotropic atomic displacement parameters for all non-hydrogen atoms, except for the atoms of some severely disordered DMF molecules in the crystal structure of **3**, which were treated isotropically. All H atoms were placed in calculated positions and refined in the riding model. Full details of the crystal structure refinement and the final structural parameters have been deposited with the Cambridge Crystallographic Data Centre (CCDC). The CCDC registry numbers and a summary of data collection and refinement parameters are provided in Table A1.

Magnetic Measurements. Magnetic properties were measured on polycrystalline samples of **1**−**3**, using a magnetic property measurement system (MPMS-XL, Quantum Design) equipped with a superconducting quantum interference device (SQUID). Magnetic susceptibility was measured in an applied DC magnetic field of 1000 Oe in the 2−300 K temperature range, under cooling and heating rates of 1 K/min. The field-dependent magnetization was measured at 1.8 K with the applied field varying from 0 to 7 T. The data were corrected for the diamagnetic contribution from the sample holder and for the intrinsic diamagnetism using tabulated constants.[47]

Transport Measurements. Electrical resistance was measured on single-crystal samples of **1**−**3**, with a typical crystal size around 0.219 × 0.209 × 0.03 mm^3 for **1**, 0.164 × 0.034 × 0.030 mm^3 for **2**, and for 0.158 × 0.123 × 0.03 mm^3 **3**. A 4-probe method was used for **1**, while the smaller size of the crystals of **2** and **3** necessitated the use of a 2-probe method. The current was applied parallel to the longer crystal's dimension, which was known to coincide with the direction of TCNQ stacks in the crystal structure. Platinum wires were attached to the crystals by using silver paint. The DC was applied by means of a Keithley 2400 source meter, while an HP 34401A multimeter was used to measure the voltage. The current bias was chosen and verified to be in the linear region of the *I-V* curves. The temperature was controlled by a ^{3}He cryostat (Oxford Cryosystems).

From 118 to 295 K, positive and negative currents were applied to the sample. The resistance was determined to be the voltage difference divided by twice the applied current. The current reversal was necessary to eliminate the thermoelectric voltages along the circuit. DC currents of ±2 nA were applied from 118 to 240 K and ±20 nA from 240 to 295 K. To ensure the veracity of the resistance measurements at low temperatures, the *I-V* curves of **1** were measured at several fixed temperatures between 60 and 111 K, in a current range from −1 nA to 1 nA. The resistance was determined from the inverse slope of the linear region of each *I-V* curve.

■ ASSOCIATED CONTENT

Supporting Information

The Supporting Information is available free of charge at https://pubs.acs.org/doi/10.1021/acs.inorgchem.1c01140.

The calculation of charges on $TCNQ^{\delta-}$ anions, thermogravimetric curves for complexes **1**−**3**, additional plots showing the crystallographic disorder model in structure **1**, a summary of X-ray data collection and crystal structure refinement parameters for **1**−**3**, the I−V curves recorded on a single crystal of **1** at various temperatures, and the dependence of the log of normalized resistance on inverse temperature for **2** and **3** (PDF)

Accession Codes

CCDC 2077064−2077066 contain the supplementary crystallographic data for this paper. These data can be obtained free of charge via www.ccdc.cam.ac.uk/data_request/cif, or by emailing data_request@ccdc.cam.ac.uk, or by contacting The Cambridge Crystallographic Data Centre, 12 Union Road, Cambridge CB2 1EZ, UK; fax: +44 1223 336033.

■ AUTHOR INFORMATION

Corresponding Author

Michael Shatruk − *Department of Chemistry and Biochemistry, Florida State University, Tallahassee, Florida 32306, United States; National High Magnetic Field Laboratory, Tallahassee, Florida 32310, United States*; Email: mshatruk@fsu.edu

Authors

Ökten Üngör − *Department of Chemistry and Biochemistry, Florida State University, Tallahassee, Florida 32306, United States*

Maylu Burrows − *Department of Chemistry and Biochemistry, Florida State University, Tallahassee, Florida 32306, United States*

Tianhan Liu − *Department of Physics, Florida State University, Tallahassee, Florida 32306, United States*; orcid.org/0000-0003-3934-0785

Michael Bodensteiner − *Department of Chemistry and Pharmacy, University of Regensburg, 93040 Regensburg, Germany*

Yuwaraj Adhikari − *Department of Physics, Florida State University, Tallahassee, Florida 32306, United States*

Zhenqi Hua − *Department of Physics, Florida State University, Tallahassee, Florida 32306, United States*; orcid.org/0000-0001-7052-3972

Brian Casas − *National High Magnetic Field Laboratory, Tallahassee, Florida 32310, United States*

Luis Balicas − *Department of Physics, Florida State University, Tallahassee, Florida 32306, United States; National High Magnetic Field Laboratory, Tallahassee, Florida 32310, United States*; orcid.org/0000-0002-5209-0293

Peng Xiong − *Department of Physics, Florida State University, Tallahassee, Florida 32306, United States*

Complete contact information is available at:

https://doi.org/10.1021/acs.inorgchem.1c01140
Inorg. Chem. 2021, 60, 10502−10512

https://pubs.acs.org/10.1021/acs.inorgchem.1c01140

Notes

The authors declare no competing financial interest.

■ ACKNOWLEDGMENTS

This research was supported by the National Science Foundation (awards CHE-1955754 to M.S. and DMR-1905843 to P.X.). B.C. and L.B. are supported by the US Department of Energy, BES program (award DE-SC0002613). The Rigaku Synergy-S single-crystal X-ray diffractometer used for crystallographic work was acquired through the NSF MRI program (award CHE-1828362). This research also used resources provided by the X-ray Crystallography Center (FSU075000XRAY) and the Materials Characterization Laboratory (FSU075000MAC) at the FSU Department of Chemistry and Biochemistry.

■ REFERENCES

(1) Coleman, L. B.; Cohen, M. J.; Sandman, D. J.; Yamagishi, F. G.; Garito, A. F.; Heeger, A. J. Superconducting fluctuations and the Peierls instability in an organic solid. *Solid State Commun.* **1973**, *12*, 1125−1132.

(2) Ferraris, J.; Cowan, D. O.; Walatka, V.; Perlstein, J. H. Electron transfer in a new highly conducting donor-acceptor complex. *J. Am. Chem. Soc.* **1973**, *95*, 948−949.

(3) Denoyer, F.; Comès, F.; Garito, A. F.; Heeger, A. J. X-ray-diffuse-scattering evidence for a phase transition in tetrathiafulvalene-tetracyanoquinodimethane (TTF-TCNQ). *Phys. Rev. Lett.* **1975**, *35*, 445−449.

(4) Jérome, D.; Mazaud, A.; Ribault, M.; Bechgaard, K. Superconductivity in a synthetic organic conductor $(TMTSF)_2PF_6$. *J. Phys., Lett.* **1980**, *41*, 95−98.

(5) Bechgaard, K.; Carneiro, K.; Rasmussen, F. B.; Olsen, M.; Rindorf, G.; Jacobsen, C. S.; Pedersen, H. J.; Scott, J. C. Superconductivity in an organic solid. Synthesis, structure, and conductivity of bis(tetramethyltetraselenafulvalenium) perchlorate, $(TMTSF)_2ClO_4$. *J. Am. Chem. Soc.* **1981**, *103*, 2440−2442.

(6) Kobayashi, H.; Cui, H.; Kobayashi, A. Organic metals and superconductors based on BETS (BETS = bis(ethylenedithio)-tetraselenafulvalene). *Chem. Rev.* **2004**, *104*, 5265−5288.

(7) Coronado, E.; Day, P. Magnetic molecular conductors. *Chem. Rev.* **2004**, *104*, 5419−5448.

(8) Fourmigué, M.; Ouahab, L. *Conducting and Magnetic Organometallic Molecular Materials*. Springer: 2009; p 193.

(9) Coronado, E.; Galán-Mascarós, J. R. Hybrid molecular conductors. *J. Mater. Chem.* **2005**, *15*, 66−74.

(10) Ouahab, L.; Enoki, T. Multiproperty molecular materials: TTF-based conducting and magnetic molecular materials. *Eur. J. Inorg. Chem.* **2004**, *2004*, 933−941.

(11) Ouahab, L. *Multifunctional Molecular Materials*. Pan Stanford Publishing: Singapore, 2013; p 289.

(12) Broderick, W. E.; Thompson, J. A.; Day, E. P.; Hoffman, B. M. A molecular ferromagnet with a Curie temperature of 6.2 K: $[Mn(C_5(CH_3)_5)_2]^+[TCNQ]^-$. *Science* **1990**, *249*, 401−403.

(13) Broderick, W. E.; Eichhorn, D. M.; Liu, X.; Toscano, P. M.; Owens, S. M.; Hoffman, B. M. Three phases of $[Fe(C_5Me_5)_2]^+[TCNQ]^-$: ferromagnetism in a new structural phase. *J. Am. Chem. Soc.* **1995**, *117*, 3641−3642.

(14) Lequan, R.-M.; Lequan, M.; Jaouen, G.; Ouahab, L.; Batail, P.; Padiou, J.; Sutherland, R. G. A new class of electrically conducting organometallic salts with an unprecedented metallocene stack. Preparation and crystal structures of η^5-cyclopentadienyl-η^6-tri- and hexa-methylbenzeneiron(II) tetracyano-*p*-quinomethanides. *J. Chem. Soc., Chem. Commun.* **1985**, *0*, 116−118.

(15) Üngör, Ö.; Shatruk, M. Transition metal complexes with fractionally charged TCNQ radical anions as structural templates for multifunctional molecular conductors. *Polyhedron* **2020**, *177*, 114254.

(16) Wang, M.; Li, Z.-Y.; Ishikawa, R.; Yamashita, M. Spin crossover and valence tautomerism conductors. *Coord. Chem. Rev.* **2021**, *435*, 213819.

(17) Ishikawa, R.; Ueno, S.; Nifuku, S.; Horii, Y.; Iguchi, H.; Miyazaki, Y.; Nakano, M.; Hayami, S.; Kumagai, S.; Katoh, K.; Li, Z.-Y.; Yamashita, M.; Kawata, S. Simultaneous spin-crossover transition and conductivity switching in a dinuclear iron(II) coordination compound based on 7,7′,8,8′-tetracyano-*p*-quinodimethane. *Chem. - Eur. J.* **2020**, *26*, 1165−1165.

(18) Clerac, R.; O'Kane, S.; Cowen, J.; Ouyang, X.; Heintz, R.; Zhao, H.; Bazile, M. J., Jr.; Dunbar, K. R. Glassy magnets composed of metals coordinated to 7,7,8,8-tetracyanoquinodimethane: M-$(TCNQ)_2$ (M = Mn, Fe, Co, Ni). *Chem. Mater.* **2003**, *15*, 1840−1850.

(19) Miller, J. S. Magnetically ordered molecule-based assemblies. *Dalton Trans.* **2006**, 2742−2749.

(20) Phan, H.; Benjamin, S. M.; Steven, E.; Brooks, J. S.; Shatruk, M. Photomagnetic response in highly conductive iron(II) spin-crossover complexes with TCNQ radicals. *Angew. Chem., Int. Ed.* **2015**, *54*, 823−827.

(21) Zhang, X.; Wang, Z.-X.; Xie, H.; Li, M.-X.; Woods, T. J.; Dunbar, K. R. A cobalt(II) spin-crossover compound with partially charged TCNQ radicals and an anomalous conducting behavior. *Chem. Sci.* **2016**, *7*, 1569−1574.

(22) Zhang, J.-Y.; Su, L.-J.; Guo, Q.-J.; Tao, J. Semiconducting spin-crossover cobalt(II) compound with non-integer charge distribution among TCNQ radicals. *Inorg. Chem. Commun.* **2017**, *82*, 39−43.

(23) Kazakova, A. V.; Tiunova, A. V.; Korchagin, D. V.; Shilov, G. V.; Yagubskii, E. B.; Zverev, V. N.; Yang, S. C.; Lin, J.-Y.; Lee, J.-F.; Maximova, O. V.; Vasiliev, A. N. The first conducting spin-crossover compound combining a Mn^{III} cation complex with electroactive TCNQ demonstrating an abrupt spin transition with a hysteresis of 50 K. *Chem. - Eur. J.* **2019**, *25*, 10204−10213.

(24) Kato, R. Conducting metal dithiolene complexes: Structural and electronic properties. *Chem. Rev.* **2004**, *104*, 5319−5346.

(25) Mori, T. Organic conductors with unusual band fillings. *Chem. Rev.* **2004**, *104*, 4947−4969.

(26) Üngör, Ö.; Phan, H.; Choi, E. S.; Roth, J. K.; Shatruk, M. Magnetism and electrical conductivity of molecular semiconductor, $[Fe^{II}(DMF)_4(TCNQ)_2](TCNQ)_2$, with fractionally charged TCNQ units. *J. Magn. Magn. Mater.* **2020**, *497*, 165984.

(27) Oshio, H.; Ino, E.; Ito, T.; Maeda, Y. Incorporation of Mn^{III} and Fe^{II} complexes into TCNQ networks: preparations, crystal structures, and magnetic properties of $[Mn^{III}(salen)(TCNQ)_{0.5}]$-$[Mn^{III}(salen)(TCNQ)_{0.5}(CH_3OH)]CH_3OH\cdot H_2O$ and $[Fe^{II}(CH_3OH)_4(TCNQ)_2]TCNQ\cdot 2CH_3CN$. *Bull. Chem. Soc. Jpn.* **1995**, *68*, 889−897.

(28) Zhao, H.; Bazile, J. M. J.; Galán-Mascarós, J. R.; Dunbar, K. R. A rare-earth metal TCNQ magnet: synthesis, structure, and magnetic properties of $\{[Gd_2(TCNQ)_5(H_2O)_9][Gd(TCNQ)_4(H_2O)_3]\}\cdot 4H_2O$. *Angew. Chem., Int. Ed.* **2003**, *42*, 1015−1018.

(29) Zhang, J.-W.; Liu, W.-H.; Li, G.-M.; Yan, P.-F.; Liu, B.-Q. Syntheses, structures, and magnetic properties of two DMTCNQ and DETCNQ gadolinium complexes. *Z. Anorg. Allg. Chem.* **2019**, *645*, 900−905.

(30) Hong, C.; Yan, P.; Li, Q.; Hou, G.; Li, G. Synthesis, structure and electrochemical properties of TCNQ lanthanide complexes. *J. Organomet. Chem.* **2013**, *739*, 45−51.

(31) Ballesteros-Rivas, M.; Zhao, H.; Prosvirin, A.; Reinheimer, E. W.; Toscano, R. A.; Valdés-Martínez, J.; Dunbar, K. R. Magnetic ordering in self-assembled materials consisting of cerium(III) ions and the radical forms of 2,5-$TCNQX_2$ (X = Cl, Br). *Angew. Chem., Int. Ed.* **2012**, *51*, 5124−5128.

(32) Zhang, J.; Yan, P.; Li, G.; Hou, G.; Suda, M.; Einaga, Y. Systematic investigation of an array of TCNQ lanthanide complexes:

synthesis, structure and magnetic properties. *Dalton Trans.* **2009**, 10466−10473.
(33) Lopez, N.; Zhao, H.; Prosvirin, A. V.; Wernsdorfer, W.; Dunbar, K. R. A homologous heterospin series of mononuclear lanthanide/$TCNQF_4$ organic radical complexes. *Dalton Trans.* **2010**, *39*, 4341−4352.
(34) Zhang, J.-W.; Wang, Y.; Yan, P.-F.; Hou, G.-F.; Li, G.-M. Solvent-directed lanthanide 7,7,8,8-tetracyano-*p*-quinodimethane complexes: syntheses, structures, magnetic and electrochemical properties. *Inorg. Chim. Acta* **2014**, *416*, 22−27.
(35) Zhang, X.; Xie, H.; Ballesteros-Rivas, M.; Woods, T. J.; Dunbar, K. R. Conducting molecular nanomagnet of Dy^{III} with partially charged TCNQ radicals. *Chem. - Eur. J.* **2017**, *23*, 7448−7452.
(36) Kistenmacher, T. J.; Emge, T. J.; Bloch, A. N.; Cowan, D. O. Structure of the red, semiconducting form of 4,4′,5,5′-tetramethyl-$\Delta^{2,2'}$-bi-1,3-diselenole-7,7,8,8-tetracyano-*p*-quinodimethane TMTSF-TCNQ. *Acta Crystallogr., Sect. B: Struct. Crystallogr. Cryst. Chem.* **1982**, *B38*, 1193−1199.
(37) Chappell, J. S.; Bloch, A. N.; Bryden, W. A.; Maxfield, M.; Poehler, T. O.; Cowan, D. O. Degree of charge transfer in organic conductors by infrared absorption spectroscopy. *J. Am. Chem. Soc.* **1981**, *103*, 2442−2443.
(38) Carlin, R. L. *Magnetochemistry*. Springer: Berlin, 1989.
(39) Lloret, F.; Julve, M.; Cano, J.; Ruiz-García, R.; Pardo, E. Magnetic properties of six-coordinated high-spin cobalt(II) complexes: theoretical background and its application. *Inorg. Chim. Acta* **2008**, *361*, 3432−3445.
(40) Benelli, C.; Gatteschi, D. Magnetism of lanthanides in molecular materials with transition-metal ions and organic radicals. *Chem. Rev.* **2002**, *102*, 2369−2388.
(41) Coulon, C.; Clerac, R. Electron spin resonance: a major probe for molecular conductors. *Chem. Rev.* **2004**, *104*, 5655−5687.
(42) Melby, L. R.; Harder, R. J.; Hertler, W. R.; Mahler, W.; Benson, R. E.; Mochel, W. E. Substituted quinodimethans. II. Anion-radical derivatives and complexes of 7,7,8,8-tetracyanoquinodimethan. *J. Am. Chem. Soc.* **1962**, *84*, 3374−3387.
(43) *CrysAlis.*; Oxford Diffraction Ltd.: Abingdon, England, 2006.
(44) *SCALE3 ABSPACK - An Oxford Diffraction program (1.0.4,gui:1.0.3)*. Oxford Diffraction Ltd.: Abingdon, England, 2005.
(45) Sheldrick, G. M. Crystal structure refinement with SHELXL. *Acta Crystallogr., Sect. C: Struct. Chem.* **2015**, *71*, 3−8.
(46) Dolomanov, O. V.; Bourhis, L. J.; Gildea, R. J.; Howard, J. A. K.; Puschmann, H. OLEX2: a complete structure solution, refinement and analysis program. *J. Appl. Crystallogr.* **2009**, *42*, 339−341.
(47) Bain, G. A.; Berry, J. F. Diamagnetic corrections and Pascal's constants. *J. Chem. Educ.* **2008**, *85*, 532−536.

https://doi.org/10.1021/acs.inorgchem.1c01140
Inorg. Chem. 2021, 60, 10502−10512